Lattice resonances in antenna arrays for liquid sensing in the terahertz regime

B. Ng,[1,3] **S. M. Hanham,**[1] **V. Giannini,**[1] **Z. C. Chen,**[2,3] **M. Tang,**[2]
Y. F. Liew,[2,3] **N. Klein,**[1] **M. H. Hong,**[2,3] **and S. A. Maier**[1,*]

[1]*Experimental Solid State Goup, Physics Department, Imperial College London, London SW7
2AZ, UK*
[2]*Department of Electrical and Computer Engineering, National University of Singapore, 4
Engineering Drive 3, 117576, Singapore*
[3]*Data Storage Institute, (A*STAR) Agency for Science, Technology and Research, 5
Engineering Drive 1, 117608, Singapore*

[*]*s.maier@imperial.ac.uk*

Abstract: Terahertz antenna arrays supporting narrow lattice resonances are proposed as an alternative sensor-on-chip approach to liquid sensing. An array of metallic rectangular antennas fabricated on a polyethylene naphthalate (PEN) substrate is used to demonstrate the sensing of a number of fluids. Good agreement is shown between experiment and simulation with Q-factors of around 20 and a figure-of-merit (FOM) of 3.80 being achieved. Liquid sensing with antenna arrays is simple both in terms of fabrication and setup. The working frequency can be tuned with a suitable choice of substrates and array parameters. The nature of the lattice resonance means that the whole sample is used to provide the conditions required for resonance occurrence, eliminating the need to preferentially locate the sample in small areas of high field concentration. The antenna arrays could also potentially be coupled with a microfluidic system for *in situ* sensing or used in a reflection setup.

OCIS codes: (240.6690) Surface waves; (260.5740) Resonance; (280.4788) Optical sensing and sensors; (300.6495) Spectroscopy, terahertz; (350.2770) Gratings.

References and links

1. S. Mickan, D. Abbott, J. Munch, X.-C. Zhang, and T. van Doorn, "Analysis of system trade-offs for terahertz imaging," Microelectron. J. **31**(7), 503–514 (2000).
2. B. Ferguson and X. C. Zhang, "Materials for terahertz science and technology," Nature Mater. **1**, 26–33 (2002).
3. M. Nagel, M. Först, and H. Kurz, "THz biosensing devices: fundamentals and technology," J. Phys. Condens. Matter **18**(18), S601–S618 (2006).
4. V. Giannini, A. Berrier, S. A. Maier, J. A. Sánchez-Gil and J. Gómez Rivas, "Scattering efficiency and near field enhancement of active semiconductor plasmonic antennas at terahertz frequencies," Opt. Express **18**(3), 2797–2807 (2010).
5. H. T. Chen, W. J. Padilla, R. D. Averitt, A. C. Gossard, C. Highstrete, M. Lee, J. F. O'Hara, and A. J. Taylor, "Electromagnetic metamaterials for terahertz applications," Int. J. Terahertz Sci. Technol. **1**(1), 42–50 (2008).
6. F. Miyamaru, S. Kuboda, K. Taima, K. Takano, M. Hangyo, and M. W. Takeda, "Three-dimensional bulk meta-materials operating in the terahertz range," Appl. Phys. Lett. **96**, 081105 (2010).
7. H. Tao, A. C. Strikwerda, K. Fan, C. M. Bingham, W. J. Padilla, X. Zhang, and R. D. Averitt, "Terahertz meta-materials on free-standing highly-flexible polyimide substrates," J. Phys. D: Appl. Phys. **41**(23), 232004 (2008).
8. R. Singh, I. A. I. Al-Naib, M. Koch, and W. Zhang, "Sharp Fano resonances in THz metamaterials," Opt. Express **19**(7), 6312–6319 (2011).
9. T. Driscoll, G. O. Andreev, D. N. Basov, S. Palit, S. Y. Cho, N. M. Jokerst, and D. R. Smith, "Tuned permeability in terahertz split-ring resonators for devices and sensors," Appl. Phys. Lett. **91**, 062511 (2007).

10. C. R. Williams, S. R. Andrews, S. A. Maier, A. I. Fernández-Domínguez, L. Martín-Moreno and F. J. García-Vidal, "Highly confined guiding of terahertz surface plasmon polaritons on structured metal surfaces," Nat. Photonics **2**, 175–179 (2008).
11. M. Navarro-Cía, M. Beruete, S. Agrafiotis, F. Falcone, M. Sorolla and S. A. Maier, "Broadband spoof plasmons and subwavelength electromagnetic energy confinement on ultrathin metafilms," Opt. Express **17**(20), 18184–181895 (2009).
12. N. Han, Z. C. Chen, C. S. Lim, B. Ng and M. H. Hong, "Broadband multi-layer terahertz metamaterials fabrication and characterization on flexible substrates," Opt. Express **19**(8), 6990–6998 (2011).
13. R. Piesiewicz, C. Jansen, S. Wietzke, D. Mittleman, M. Koch, and T. Kürner, "Properties of building and plastic materials in the THz range," Int. J. Infrared Millim. Waves **28**(5), 363–371 (2007).
14. T. Ikeda, A. Matsushita, M. Tatsuno, Y. Minami, M. Yamaguchi, K. Yamamoto, M. Tani, and M. Hangyo, "Investigation of inflammable liquids by terahertz spectroscopy," Appl. Phys. Lett. **87**, 034105 (2005).
15. P. U. Jepsen, U. Mø ller, and H. Merbold, "Investigation of aqueous alcohol and sugar solutions with reflection terahertz time-domain spectroscopy," Opt. Express **15**(22), 14717–14737 (2007).
16. M. Brucherseifer, M. Nagel, P. H. Bolivar, H. Kurz, A. Bosserhoff, and R. Buttner, "Label-free probing of the binding state of DNA by time-domain terahertz sensing," Appl. Phys. Lett. **77**(24), 4049 (2000).
17. M. Nagel, P. H. Bolivar, M. Brucherseifer, H. Kurz, A. Bosserhoff, and R. Buttner, "Integrated THz technology for label-free genetic diagnostics," Appl. Phys. Lett. **80**(1), 154 (2002).
18. C. Debus and P. H. Bolivar, "Frequency selective surfaces for high sensitivity terahertz sensing," Appl. Phys. Lett. **91**, 184102 (2007).
19. Y. Sun, X. Xia, H. Feng, H. Yang, C. Gu, and L. Wang, "Modulated terahertz responses of split ring resonators by nanometer thick liquid layers," Appl. Phys. Lett. **92**, 221101 (2008).
20. T. Baras, T. Kleine-Ostmann, and M. Koch, "On-chip THz detection of biomaterials: a numerical study," J. Biol. Phys. **29**(2), 187–194 (2003).
21. R. E. Collins and F. J. Zucker, *Antenna Theory Part 1* (McGraw-Hill Inc., 1969).
22. R. E. Collins and F. J. Zucker, *Antenna Theory Part 2* (McGraw-Hill Inc., 1969).
23. B. Auguié and W. Barnes, "Collective resonances in gold nanoparticle arrays," Phys. Rev. Lett. **101**, 143902 (2008).
24. G. Vecchi, V. Giannini, and J. Gómez Rivas, "Surface modes in plasmonic crystals induced by diffractive coupling of nanoantennas," Phys. Rev. B **80**, 201401 (2009).
25. G. Vecchi, V. Giannini, and J. Gómez Rivas, "Shaping the fluorescent emission by lattice resonances in plasmonic crystals of nanoantennas," Phys. Rev. Lett. **102**, 146807 (2009).
26. V. Giannini, G. Vecchi, and J. Gómez Rivas, "Lighting up multipolar surface plasmon polaritons by collective resonances in arrays of nanoantennas," Phys. Rev. Lett. **105**, 266801 (2010).
27. V. A. Markel, "Coupled-dipole approach to scattering of light from a one-dimensional periodic dipole structure," J. Mod. Opt. **40**(11), 2281–2291 (1993).
28. V. A. Markel, "Divergence of dipole sums and the nature of non-Lorentzian exponentially narrow resonances in one-dimensional periodic arrays of nanospheres," J. Phys. B **38**, L115–L121 (2005).
29. S. Zou, N. Janel, and G. C. Schatz, "Silver nanoparticle array structures that produce remarkably narrow plasmon lineshapes," J. Chem. Phys. **120**(23), 10871–10875 (2004).
30. L. J. Sherry, S. H. Chang, G. C. Schatz, R. P. Van Duyne, B. J. Wiley, and Y. Xia, "Localized surface plasmon resonance spectroscopy of single silver nanocubes," Nano Lett. **5**(10), 2034–2038 (2005).
31. L. Duvillaret, F. Garet, and J.-L. Coutaz, "A reliable method for extraction of material parameters in terahertz time-domain spectroscopy," IEEE J. Sel. Top. Quantum Electron. **2**(3), 739–746 (1996).
32. R. M. Cole, S. Mahajan, and J. J. Baumberg, "Stretchable metal-elastomer nanovoids for tunable plasmons," Appl. Phys. Lett. **95**, 154103 (2009).
33. I. M. Pryce, K. Aydin, Y. A. Kelaita, R. M. Briggs, and H. A. Atwater, "Highly strained compliant optical metamaterials with large frequency tunability," Nano Lett. **10**(10), 4222–4227(2010).
34. C. Y. Chen, I. W. Un, N. H. Tai, and T. J. Yen, "Asymmetric coupling between subradiant and superradiant plasmonic resonances and its enhanced sensing performance," Opt. Express **17**(17), 15372–15380 (2007).

1. Introduction

The main issue that prevents the widespread use of terahertz (THz) radiation, despite its interesting properties in spectroscopy, imaging and bio-sensing, is the lack of high powered sources and sensitive detectors [1–3]. One particularly interesting aspect of THz wave research is sensing, because THz frequencies correspond to the rotational and vibrational modes of both simple and complex biomolecules. However due to the lack of high-powered sources and sensitive detectors, researchers have been forced to look to other avenues to improve sensitivities for molecular detection [4]. One proposal lies in the use of metamaterials which allows for the en-

gineering of the photonic response and high field concentrations via structured subwavelength elements [5–12].

Although much effort has been devoted to applying THz waves to the sensing and characterisation of a wide range of materials like building materials [13], inflammable liquids [14], sugar solutions [15] and DNA [16, 17], there is still a demand for a simple, cheap and disposable sensor-on-chip type of approach to THz sensing [3] in order to enable widespread adoption of THz sensing methods. Attempts to meet this demand have taken the form of split-ring resonator (SRR) metamaterials [8,9,18,19] and waveguide-like sensors [3,17,20]. However these approaches generally involve complex setups and fabrication procedures and may require the sample to be preferentially located at positions of high field concentrations.

In this article, an optical phenomenon which couples the diffractive modes of a 2D grating of antennas to the geometrical resonance modes of the individual antennas is investigated in the context of liquid sensing [21–26]. Such coupling has previously been demonstrated in the optical regime, where by using a 2D array of rectangular antennas a sharp tunable resonance has been observed [23–26]. Here, such a coupling effect is scaled up to the THz regime and applied to detect changes in the refractive indices of fluids placed on the antenna array. This proposed approach of utilizing diffractive coupling is simple in terms of both fabrication and setup. It can also be used as a disposable sensor. Most importantly, the working frequency regime can be tuned by adjusting structural parameters on the chip.

2. Theory

Consider a periodic 1D chain of dipole-like spheres in vacuum with radius a, and lattice constant h, illuminated normally by light polarized in a direction perpendicular to the chain axis. As given by Markel [27, 28], the dipole amplitude of particle m, d_m, taking into account the incident light and the radiated fields of the other dipoles in the chain is given by

$$d_m = \alpha \left[E_0 + \sum_{m' \neq m} W_{m-m'}(kh) d_{m'} \right], \tag{1}$$

where $k = 2\pi/\lambda$ is the incident wavevector, m and m' are the dipole indices, α is the polarizability of the dipole, E_0 is the incident field and $W_p(x) = k^3 \left(x^{-1}/|p| + ix^{-2}/|p|^2 - x^{-3}/|p|^3 \right) \exp(ix|p|)$ is the dipole interaction term in which $p = m - m'$ and $x = kh$.

Solving Eq. 1 gives an *effective* dipole amplitude for such a particle in the chain [28]

$$d_m = \frac{a^3 E_0}{a^3/\alpha - (ka)^3 S(kh)}, \tag{2}$$

where $S(x) = 2 \sum_{m>0} (1/xm + i/(xm)^2 - 1/(xm)^3) \exp(imx)$ encapsulates the dipole interactions from the chain elements.

When the wavelength of the incident light is close to the lattice constant of the chain, there is a resonance in d_m and a partial cancellation in the radiative damping of the dipoles [29]. (For a detailed theoretical analysis, see [28,29].) As a result, there is a narrow dip in transmission caused by the coupling of the diffractive modes to the dipole resonances of the individual particles. This resonance is a *collective* mode which is due to the periodicity of the chain and the interaction between the dipoles. This theoretical framework in one dimension can be extended to describe a 2D grating as well [23,29]. In this paper, the *collective* mode will be referred to as the lattice resonance as in [24,25].

3. Experimental and Simulation Methods

2D arrays of rectangular metal antennas were fabricated via direct femtosecond laser writing followed by a lift-off process on $100\,\mu m$ thick polyethylene naphthalate (PEN) substrates obtained from Dupont Teijin Films (Teonex Q81). PEN was chosen because its refractive index is around 1.8, which is quite close to those of the samples used in this work. With a smaller refractive index difference between the substrate and the sample, as will be explained later in Sec. 4, a stronger lattice resonance could be obtained. Additionally, PEN is an inexpensive and durable material. The PEN substrate was first spin coated with $2.2\,\mu m$ of Microposit S1822 positive tone photoresist at $5000\,RPM$ and baked on a hotplate for 1 minute at $110°C$. The sample was then placed on a precision nanopositioning stage with computer numerical control (CNC) and exposed to light generated by a frequency doubled Ti:Sapphire femtosecond laser (Spectra Physics Tsunami, Model 3960, $\lambda = 400\,nm$, $\tau = 100\,fs$, repetition rate = $82\,MHz$). The light is focussed onto the sample via a microscope objective ($100\times$, $NA = 0.7$). The antenna patterns were written on the photoresist by controlling the stage movement through CNC and exposure via a shutter. Development of the sample was done with Microposit MF-319 developer to remove the exposed photoresist, revealing the inverse antenna array. Electron beam evaporation was used to deposit $5\,nm$ of Cr followed by $200\,nm$ of Au on the sample. The thin Cr layer acts to improve the adhesion of the Au film to the PEN substrate. Lastly, acetone ultrasonic agitation was used to remove any unwanted photoresist and metallic film, leaving behind the antenna array as shown in Fig. 1(a). A 30×30 array consisting of $(85 \pm 1)\,\mu m \times (38 \pm 3)\,\mu m$ Au antennas was fabricated with periods of $P_x = (200 \pm 1)\,\mu m$ and $P_y = (221 \pm 1)\,\mu m$ in the x- and y-direction, respectively as shown in Fig. 1(a). The entire sample measures approximately $6\,mm \times 6.6\,mm$ which is sufficiently big to ensure that the entire THz beam (beam diameter, $d_{beam} \approx 2\,mm$) is within the sample area and any collective behaviour amongst the antennas of the array is well captured.

The THz antenna arrays were characterized using a terahertz time-domain spectrometer (THz-TDS) (TPS3000, TeraView Inc.). The time domain results were Fourier transformed to give the frequency domain spectra. In order to make measurements with fluids on the THz antenna array, a $50\,\mu m$ spacer was placed on the array substrate to create a chamber to hold the fluid. A $100\,\mu m$ thick PEN superstrate was then placed over the chamber (see Fig. 1(c)). The entire chamber assembly was then placed at the focal point of the THz beam so that the THz light generated was normally incident, polarized in the x-direction (Fig. 1(b)). Measurements were made with gaseous nitrogen, methanol, ethanol and liquid paraffin in the fluid chamber at room temperature. For all the fluids, a reference spectrum was measured by taking the transmission spectrum of the fluid chamber, seen in Fig. 1(c), without any THz antenna array. All measurements were taken in a nitrogen purged chamber. A Figure-of-Merit (FOM), as defined by Eq. 3 [30], was then extracted from the experimental data.

$$FOM = \frac{\Delta\lambda_{res}/\Delta n}{\Gamma},$$ (3)

where $\Delta\lambda_{res}$ is the change in resonance wavelength, Δn is the change in refractive index and Γ is the full width at half maximum (FWHM) of the resonance.

Simulations for $200\,\mu m < \lambda < 600\,\mu m$ (i.e. 0.5 THz to 1.5 THz) were carried out using the finite-difference-time-domain (FDTD) method (FDTD Solutions 6.5, Lumerical Inc.) by applying periodic boundary conditions to a unit cell containing one antenna. The antenna was assumed to be a perfect electric conductor (PEC) with rounded ends and has dimensions of $l = 85\,\mu m$, $w = 38\,\mu m$ and a thickness of $200\,nm$. THz antenna arrays embedded in a homogeneous environment of $n = 1.7$ were first investigated. This is because the diffractive coupling is most efficient in a homogeneous environment and spectrum artifacts due to substrates and
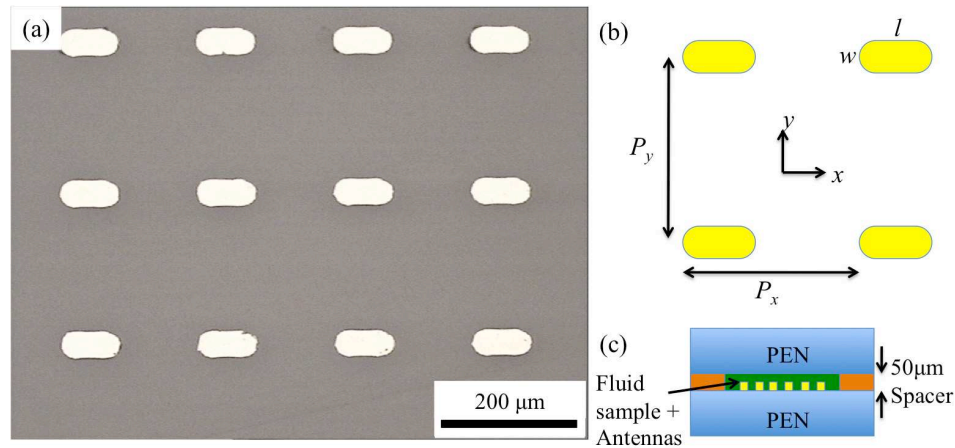
Fig. 1. (a) Optical microscope image of THz antenna array. (b) Schematic diagram of THz antenna array with antennas of length l, width w and periods P_x and P_y in the x and y directions, respectively. (c) Schematic diagram of the fluid chamber assembly used for transmission measurements.

superstrates can be cut out to give a clear picture of the lattice resonance [24, 25]. Finally, simulations with actual fluid refractive indices were performed to match simulations with experiments as well. The fluid chamber seen in Fig. 1(c) was included in these simulations. The liquid refractive indices were retrieved from transmission measurements using methods detailed in [31] and the refractive index of nitrogen was assumed to be 1.00.

4. THz Antenna Arrays in a Homogeneous Environment

An infinite antenna array with antenna dimensions specified in Sec. 3 embedded in an infinite homogeneous environment with $n = 1.7$ was simulated. The transmission spectrum is shown in Fig. 2(a). First of all, grating features like the $(0,1)$ and $(1,1)$ Rayleigh anomalies can be clearly seen (blue dashed lines in Fig. 2 show the theoretical positions of the Rayleigh anomalies). The $(1,0)$ Rayleigh anomaly is not clearly resolved due to the symmetry of the system [26]. The broad dip at $281\,\mu m$ (Fig. 2(a), red square) corresponds to the half-wavelength geometrical resonance of the individual antenna. At $\lambda = 389\,\mu m$ (Fig. 2(a), green circle), a sharp lattice resonance as a result of the interactions described in Sec. 2 is seen. The position of the lattice resonance is close to the point where $\lambda \approx 1.7P_y$ in accordance to theory. The resonance has its narrow and deep nature because 1) the phase matching conditions only occur in a narrow frequency range, and 2) the effect is a cumulative effect incurred by the interaction of many antennas. Note also that the lattice resonance is related to the periodicity of the system and the geometrical resonance mode of the antenna. This means that the working frequency can be tuned simply by adjusting the lattice parameters and antenna length. Previous work at optical frequencies suggests the possibility of tuning the lattice parameters via mechanical stretching or compression [32,33].

Figs. 2(b) and (c) show the log-scale electric field intensity distribution in the z-normal plane at the antenna dipole resonance ($\lambda = 281\,\mu m$) and the lattice resonance ($\lambda = 389\,\mu m$), respectively. The entire cross section of the unit cell is captured within the field distribution plots. The geometrical half-wavelength mode of the antenna results in a dipole-like field distribution as depicted in Fig. 2(b). At the lattice resonance (Fig. 2(c)), one gets a delocalized field distribution where the field intensity is enhanced in almost the whole unit cell. There is also an
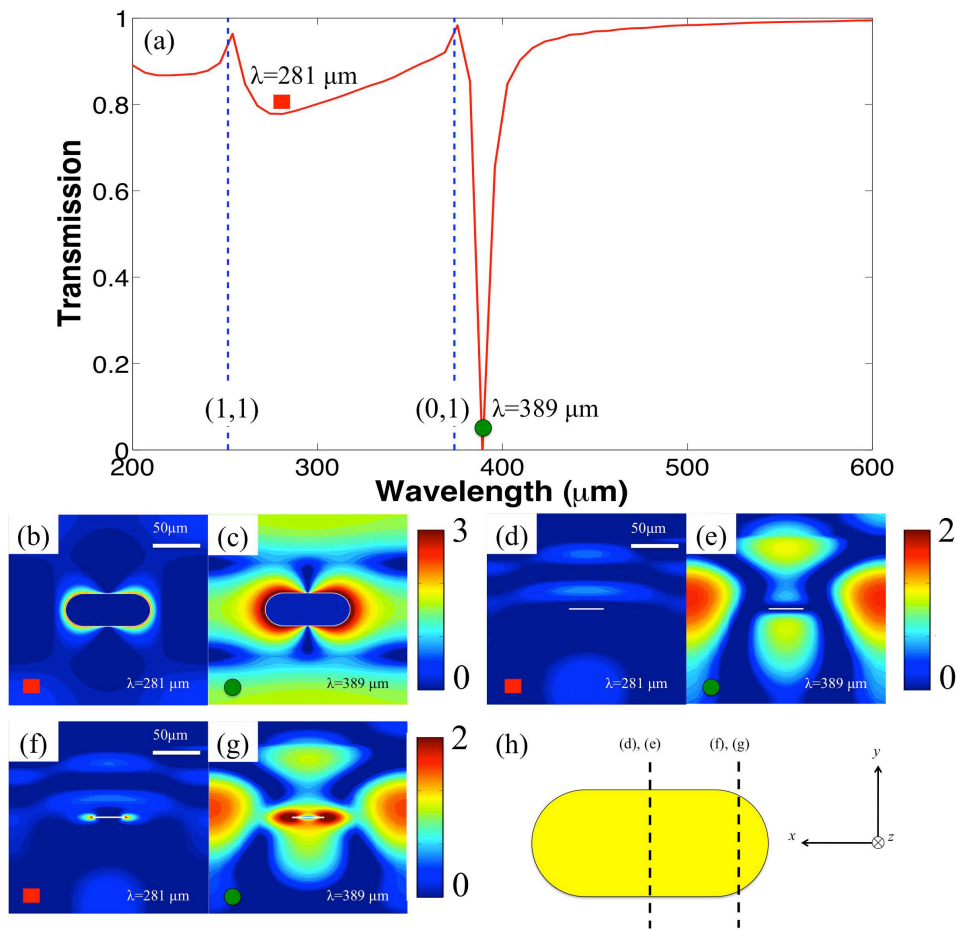
Fig. 2. (a) Simulated transmission spectrum of the THz antenna array ($l = 85\,\mu m$, $w = 38\,\mu m$, $P_x = 200\,\mu m$ and $P_y = 220\,\mu m$) embedded in an infinite homogeneous medium of $n = 1.7$. (0,1) and (1,1) Rayleigh anomalies (blue dashed lines) occur at $\lambda = 374\,\mu m$ and $\lambda = 251\,\mu m$, respectively. The geometrical dipole resonance (red square) and the lattice resonance (green circle) can also be clearly seen. (b, c) Log-scale electric field intensity distributions in the z-normal plane at $\lambda = 281\,\mu m$ and $\lambda = 389\,\mu m$. (d − g) Log-scale electric field intensity distributions in the x-normal plane cutting through the center of the antenna ((d) and (e)) and at $32.5\,\mu m$ offset from the center in the x-direction ((f) and (g)) at $\lambda = 281\,\mu m$ and $\lambda = 389\,\mu m$. The white line marks out the antenna position. (h) Diagram indicating the coordinate system and the cutting planes of (d, e) and (f, g).

enhanced electric field intensity between the antennas in the y-direction, indicating a coupling in the y-direction of the diffractive mode and the antenna mode. This is further confirmed by looking at the electric field intensity distributions in the x-normal plane cutting through the antenna at its center (Figs. 2(d) and (e)) and at a $32.5\,\mu m$ offset from the center (Figs. 2(f) and (g)), which show that the field intensities between the antennas in the coupling direction at the lattice resonance are enhanced as compared to that at the half wavelength resonance of the antenna (See Fig. 2(h) for diagram indicating cutting planes). From the perspective of liquid

sensing, this has two very important benefits. Firstly, the enhanced polarizability of the antenna increases the interaction with the sample. Secondly, the antenna array in a sense *probes* the whole sample since the entire sample area is used to provide the phase matching conditions for the lattice resonance to occur. This means that the entire sample is utilized for sensing in contrast to the case for metamaterials where only the samples located in the electric field *hot spots* are effectively detected [18].

At this point, it is to be noted that the case presented above is an idealized one where the antennas are embedded in a homogeneous and lossless dielectric environment. In experiments, the presence of loss and refractive index differences between substrate and fluid samples will affect the lattice resonance. The strength of the lattice resonance depends on the ability of the diffracted light to propagate along the surface to interact with other antennas. The presence of loss causes the diffracted light to attenuate as it propagates and refractive index differences result in the de-phasing of the surface wave. This means that an individual antenna will not interact with all the antennas in the array but only with neighboring antennas within a given range. Thus the contribution of the second term in the square brackets of Eq. 1 will be diminished, leading to a weaker lattice resonance. Nonetheless, it is still possible to have a good interaction over several lattice constants as long as the substrate is suitably chosen [24].

5. THz Antenna Arrays for Liquid Sensing

The experimental and simulated transmission spectra for nitrogen, liquid paraffin, ethanol and methanol are shown in Figs. 3 (a – d) respectively. As can be seen, there is good qualitative agreement between the experimental (red solid lines) and simulated (black dashed lines) spectra. The lattice resonance is marked out by the red arrow. In Fig. 3(a), the lattice resonance for nitrogen is weaker than those of the liquid samples. This is mainly due to the refractive index difference between the PEN substrate and nitrogen, which results in a de-phasing of the surface mode. The dips prior to the lattice resonance are guided modes that exist within the substrate or superstrate due to phase matching from the periodicity of the array. Another feature of the spectra is that the geometrical half wavelength resonance of the antennas in Fig. 2(a) is obscured by the guided mode resonances. Although at some points the guided mode resonance seems to be sharper than the lattice resonance (for example, the dip at $\lambda \approx 300\,\mu m$ in Fig. 3(b)), such guided mode resonances are not suitable for sensing purposes as they may depend critically on the sample or substrate thicknesses and refractive indices and may exhibit cutoff behavior. In comparison, the lattice resonance is mainly sensitive to the array parameters, making it more robust for sensing purposes since variances in sample thickness and refractive index are unlikely to cause the lattice resonance to disappear completely. The guided modes can be moved out of the desired frequency regime by using a suitably thin substrate and superstrate.

The resonant wavelengths λ_{res}, and the corresponding fluid refractive index n_{res}, for the characterized fluids are shown in Table 1. As can be seen, the lattice resonance wavelength changes with the refractive index of the fluid sample as a result of changes in the phase matching conditions. This demonstrates that the antenna arrays, utilizing diffractive coupling, are sensitive to the refractive index of the fluid environment.

The Q-factor of the THz antenna array is around 20 which is almost double that reported for SRR metamaterials [9] (Q-factor $\approx$ 10) and at least comparable to that in asymmetric SRRs supporting Fano resonances [8]. This points to potential sensing applications for the THz antenna array. In order to quantitatively investigate the viability of THz antenna arrays as liquid sensors, a figure-of-merit (FOM) defined by Eq. 3 is calculated. Fig. 4 shows the change in lattice resonance wavelength $\Delta\lambda_{res}$ plotted against the refractive index of the fluid n_{res} at λ_{res}. As can be seen, the data is well-described by the linear fit equation $\Delta\lambda_{res} = 70.73 n_{res} - 70.82$. Using Eq. 3, the FOM is calculated to be 3.80. The closest comparison to the best of our knowl-

Table 1. Table of Lattice Resonance Wavelength λ_{res} and Corresponding Refractive Index n_{res} for Nitrogen, Liquid Paraffin, Ethanol, and Methanol

Fluid Sample	Resonance Wavelength, λ_{res} (μm)	Refractive Index n_{res}, at λ_{res}
Nitrogen	367	1.00
Liquid Paraffin	400	1.49
Ethanol	412	1.60
Methanol	416	1.71
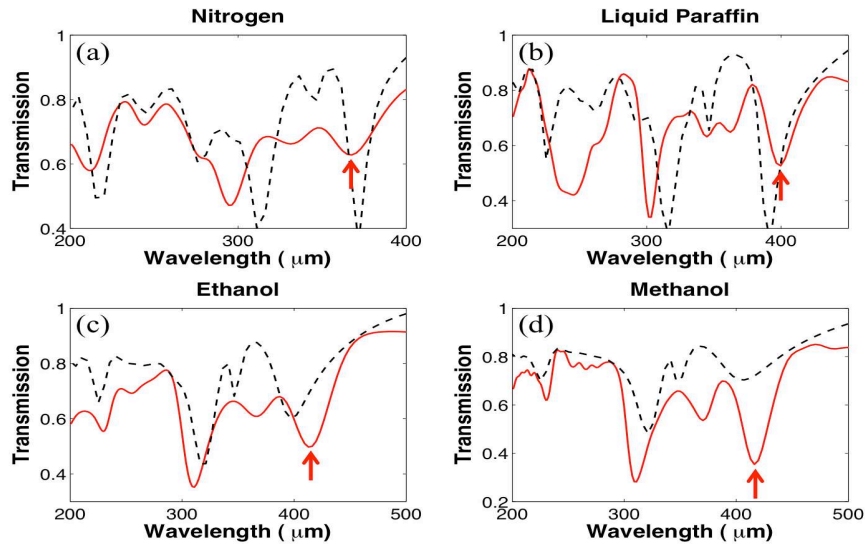
Fig. 3. (a – d) Experimental (red solid lines) and simulated (black dashed lines) transmission spectra for nitrogen, liquid paraffin, ethanol and methanol, respectively. The lattice resonance is marked by the red arrow. Transmission dips at wavelengths smaller than that of the lattice resonance is due to guided modes that exist in the substrate and superstrate.

edge is for sensing in the mid-IR regime where the highest FOM calculated from simulation results was 2.86 [34].

One would expect that the lattice resonance strength would increase if the beam diameter, d_{beam} is larger and the number of antennas illuminated is increased. However, in the limit of the interaction length of the surface mode, L_x, being much smaller than the illuminated area, $L_x <<$ d_{beam}, any increase in d_{beam} would not add significantly to the lattice resonance strength. L_x was calculated using the method described in [24] for the case of nitrogen to estimate whether the lattice resonances in our experiments can be strengthened. It was found that L_x is approximately $1.2\,mm$. Given that d_{beam} is approximately $2\,mm$, it is expected that a larger THz beam spot would lead to a stronger lattice resonance. This can be seen from the simulation results of the nitrogen sample where a stronger lattice resonance results from an infinite array illuminated by a plane wave.

The THz antenna array offers a cheap and simple approach to liquid sensing. Fabrication can be done with industrially accessible materials and photolithography methods like mask lithography, microlens array lithography and direct-laser writing to make it viable for disposable sensor-on-chip detection. A standard transmission spectroscopy setup is used as compared
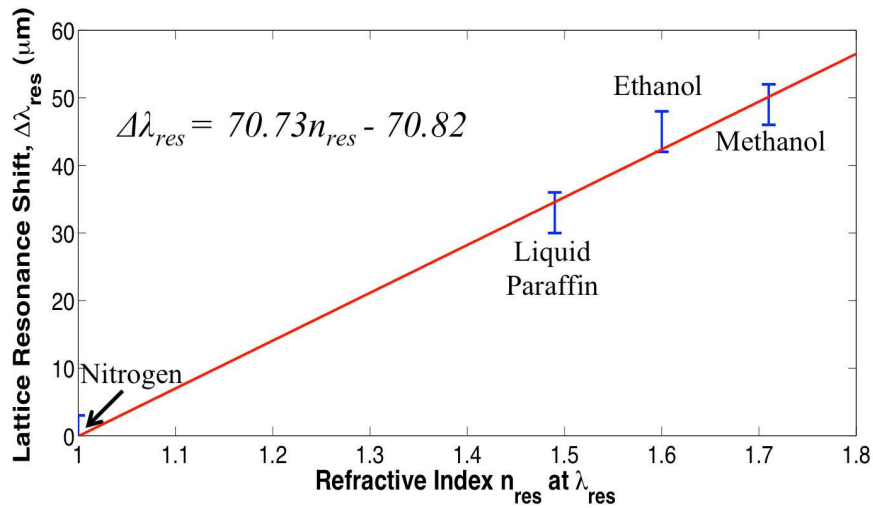
Fig. 4. Lattice resonance shift, $\Delta\lambda_{res}$ plotted against the refractive index n_{res} at λ_{res}. The data is well described by the equation $\Delta\lambda_{res} = 70.73n_{res} - 70.82$ (red line) for $50\,\mu m$ thick samples.

to the more complex setup required in [3, 17, 20]. Phase matching for the lattice resonance is provided by the *whole* sample thus reducing the need to localise the sample in specific areas. Another benefit of *probing* the entire sample is that smaller sample volumes would be required for effective sensing as compared to conventional cuvette based transmission measurements. This approach could potentially be coupled with a microfluidic system for *in situ* sensing or used in a reflection setup to reduce the effect of losses due to transmission through the sample.

6. Conclusion

Metallic antenna arrays are proposed as an alternative method to realize liquid sensing in the THz regime. The arrays support narrow lattice resonances that are due to the coupling of the diffractive modes of the grating to the geometrical resonance modes of the individual antennas when phase matching conditions are met. The nature of the resonance means that the whole sample is used to provide the resonance conditions necessary. Sensing of nitrogen, liquid paraffin, ethanol and methanol are performed with good match to the simulations. High Q-factors of around 20 and a FOM of 3.80 are achieved. The antenna array presented here is simple in terms of fabrication and setup, tunable and potentially applicable to *in situ* and reflection mode sensing.

Acknowledgments